Electronic Supplementary Material (ESI) for CrystEngComm.

Supporting Information for

Highly Varied Reaction Cavities within a Single Molecular Crystal

Michael R. Carr[a], Matthew Kochert[a], Wathsala L. I. Waduge[b], Gregory J. Deye[a], Kenneth W. Olsen[a], and Jacob W. Ciszek*[a]

---

[a] Department of Chemistry and Biochemistry, Loyola University Chicago,
Chicago, Illinois, 60660, United States E-mail: jciszek@luc.edu
[b] Department of Chemistry and Biochemistry, Illinois Wesleyan University,
Bloomington, Illinois, 61701, United States

Table of Contents

Experimental Conditions

Crystal Growth

Tetracene crystal growth was performed using a home-built tube furnace[1] with the source temperature set at 202-203°C. Under an inert argon atmosphere (flow rate = 40 cm^3/min), crystals were deposited on silicon wafers placed between 15 cm and 27 cm downstream from the highest temperature location in the tube. The crystals were grown over a 48 h period before the wafers were removed.

Diels-Alder Reaction

The wafer containing the tetracene crystals was placed in a Schlenk tube opposite ~10 mg of reactant. The tube was evacuated followed by replacement with nitrogen gas. This process was repeated an additional two more times before the tube was placed in an oven and allowed to react at 40°C for 8 h or 16 h. After the reaction, the sample side of the tube was kept warm while the opposite end was cooled using dry ice for 2 min to condense any residual reactant vapors. The tetracene wafer was removed and placed under high vacuum ($<10^{-4}$ Torr) for 1 h.

SEM and EDX

After the reaction, vertical, potentially indexable, crystals were identified using a Hitachi SU3500 SEM and EDX data was acquired via a Bruker XFlash Detector 630M EDX. SEM/EDX was selected for analysis because it allows both imaging (SEM) and quantification (EDX) in a single system which overcomes the throughput constraints inherent in the experiment. EDX has an angular dependence and thus crystals were selected to be vertical (not deviating more than ~20° from the surface normal) and thicker than ~5 μm to assure that the electron beam generated sufficient signal to be measurable before degradation. EDX was performed on crystals first, rather than indexing, to minimize the amount of oxidation induced by the beam. The horizontal facet was scanned for 20-300 s to maintain similar surface total counts across analyzed crystals, which kept the signal to noise similar over crystal facets of different sizes. The maximum time crystals were exposed to the beam was below 300 s, which typically gave less than 1% oxidation. The resulting spectra were analyzed using the Quantax Esprit software using a ZAF quantification model with background setting ranges of 0.37685-0.41685 keV and 0.60685-0.76685 keV. Crystals were subsequently imaged for indexing.

Indexing

Scanned crystals needed defined facets and to be free of major imperfections to allow for successful indexing. Crystals were manipulated using the SEM stage's rotate and tilt capabilities to image the largest facet of the crystal, which corresponds to either the (001) or $(00\bar{1})$ crystallographic plane. The angles formed on the major facet as well as the angles formed on the minor facets were measured using the ImageJ software, and were compared to the angles formed on a model tetracene crystal depicted using the KrystalShaper software in order to assign a Miller Index to the scanned surface. A subset of tilted crystals were also rotated to generate a side view, which allowed all angles associated with the crystal facet to be measured and corroborated.

Reactivity Analysis

The reaction at the $(11\bar{1})$ crystallographic plane was excluded as the larger relative error for that particular measurement meant any trend was statistically meaningless. The remaining crystallographic planes ((001), $(1\bar{1}0)$, $(1\bar{1}\bar{1})$, $(1\bar{1}1)$, and (110)) had a minimum of three crystals that were measured at the two time points at which initial kinetics were probed (8 h and 16 h). Longer reaction times were initially performed, but discontinued as the majority of surfaces showed no further increase in product (Figure S1) and because analysis of equilibrium states can be complicated by surface reorganization or potential retro-Diels-Alder reaction. For the five surfaces that met the minimum requirements, weighted mean and weighted standard deviation for the oxygen percentage were calculated and are given in Table 1. The weights for each value were determined using the absolute error that accompanied each scan. The absolute error describes the error in measurement expected from the counting statistics used by the EDX software, so by using it to determine weights, greater import was given to values with higher confidence intervals.

Molecular Dynamic Simulations

The starting structure for the tetracene (TETCEN) surface (obtained from the Cambridge Structural Database)[2] was generated using Mercury.[3] The simulation box containing these tetracene surfaces as well as the maleic anhydrides were generated using VMD.[4] Molecular dynamics simulations were then performed on these simulation boxes using NAMD.[5] The MD simulations involved a short energy minimization (3000 steps) followed by unrestrained dynamics for 10 ns. Periodic boundary conditions were applied to the system. A distance of 15 Å was used for the cutoff for nonbonding (electrostatic and van der Waals) interactions. A 1.0 1-4 scaling factor was used and the switch distance was 13 Å. The temperature was set to 303 K. The time step was 2 fs with every 150th step in the trajectory saved for analysis.

Energy Minimizations

Interaction energies between a representative maleic anhydride and the surface were calculated for all frames of the MD simulations. An energy minimization was then performed on two frames with low and high initial interaction energies from the MD simulations of the (110), $(1\bar{1}0)$, $(1\bar{1}1)$ and $(1\bar{1}\bar{1})$ surfaces. These systems then underwent an energy minimization of 6000 steps with the same aforementioned conditions. All calculations were performed using CHARMM 36 parameters.[6–9]

Average EDX Data for All Facets

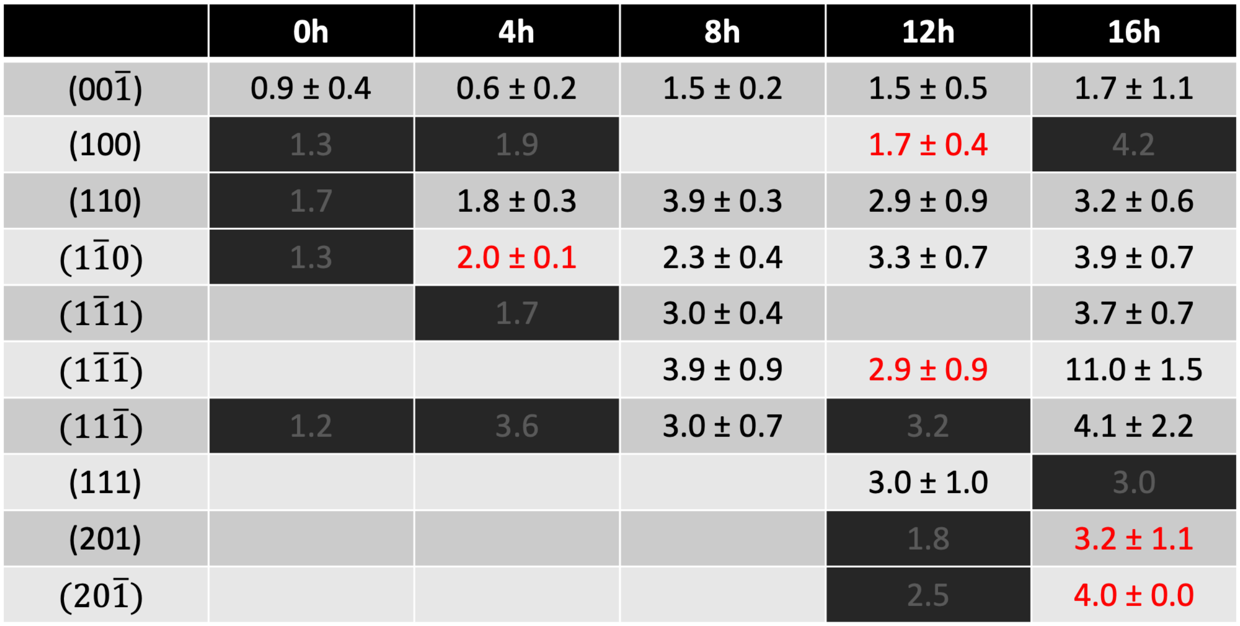

	0h	4h	8h	12h	16h
$(00\bar{1})$	0.9 ± 0.4	0.6 ± 0.2	1.5 ± 0.2	1.5 ± 0.5	1.7 ± 1.1
(100)	1.3	1.9		1.7 ± 0.4	4.2
(110)	1.7	1.8 ± 0.3	3.9 ± 0.3	2.9 ± 0.9	3.2 ± 0.6
$(1\bar{1}0)$	1.3	2.0 ± 0.1	2.3 ± 0.4	3.3 ± 0.7	3.9 ± 0.7
$(1\bar{1}1)$		1.7	3.0 ± 0.4		3.7 ± 0.7
$(1\bar{1}\bar{1})$			3.9 ± 0.9	2.9 ± 0.9	11.0 ± 1.5
$(11\bar{1})$	1.2	3.6	3.0 ± 0.7	3.2	4.1 ± 2.2
(111)				3.0 ± 1.0	3.0
(201)				1.8	3.2 ± 1.1
$(20\bar{1})$				2.5	4.0 ± 0.0

***Figure S1**: Complete data table of average oxygen percent for each facet found and reacted with maleic anhydride for the given time frame. Red data has only two values providing tentative information on a particular surface, but are not reported in the main text.   Blacked out boxes are for data from a single crystal facet and were excluded from analysis. Main text data comes from a minimum of 3 crystals, more commonly 4 or 5.*

EDX Quantification of *N*-methylmaleimide Reactions

Facet	O%	N%	Ratio
$(\bar{1}\bar{1}0)$	2.9 ± 0.3	1.2 ± 0.3	2.4 ± 0.8
$(1\bar{1}0)$	1.9 ± 0.2	0.9 ± 0.2	2.0 ± 0.5
(111)	1.7 ± 0.2	1.5 ± 0.2	1.1 ± 0.2
(110)	3.0 ± 0.2	1.3 ± 0.1	2.3 ± 0.4

Average Ratio = 2.0 ± 0.6

***Figure S2**: EDX analysis of a 16 h Diels-Alder reaction with N-methylmaleimide. The ratio was calculated by dividing the oxygen percent by the nitrogen percent. Ratios higher than a 2:1 would demonstrate oxygen signal brought on by oxidation of the tetracene surface.*

Discussion of $(1\bar{1}\bar{1})$ surface's saturation.

Though tangential to the kinetic discussion, the saturation should be addressed. The saturation point of 3.5-4% surface oxygen corresponds to ~2 layers of adduct which is probably the most that can react without major rearrangement. The fact that the $(1\bar{1}\bar{1})$ surface saturates at a much higher level than this necessitates significant surface reorganization and the fact that none of the other surfaces showed rearrangement is puzzling. We presume that the relatively high surface density combined with tetracene's orientation near parallel to the surface might result in the need to relieve chemical pressure via such a rearrangement. Unfortunately, detailed analysis of this phenomenon is well beyond the scope of this paper.

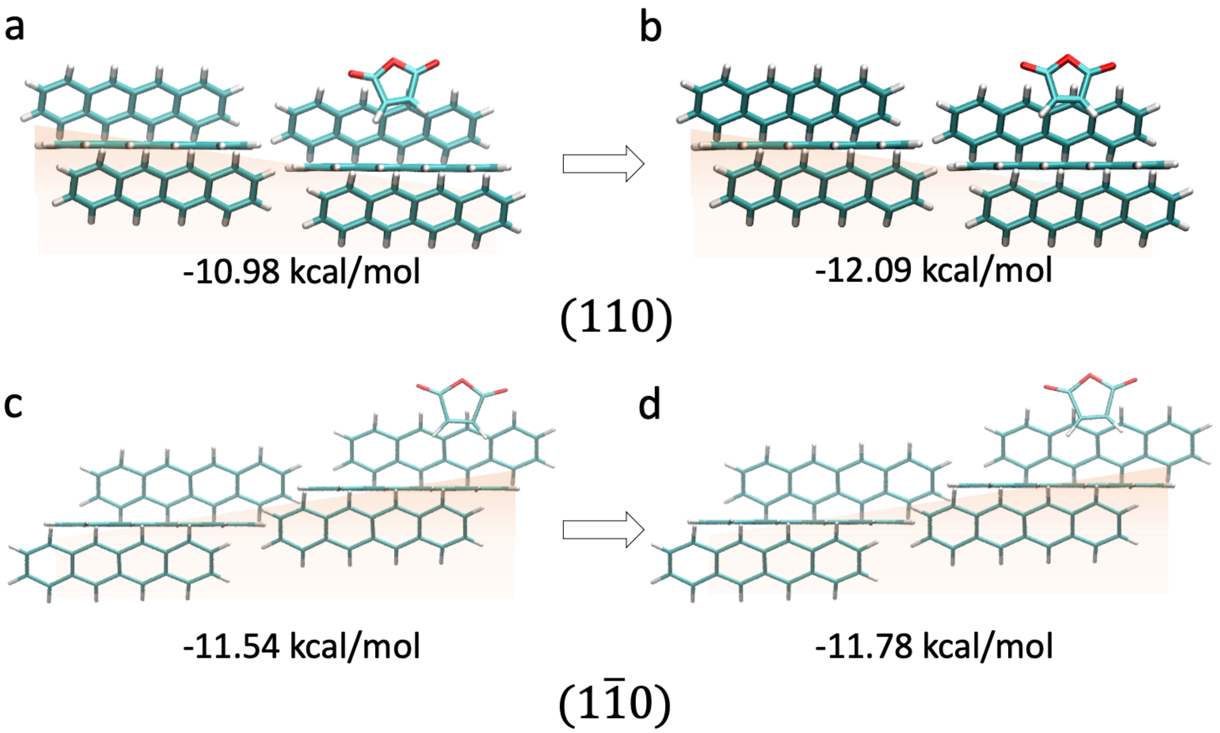

Figure S3: Representative energy minimized structures of tetracene $(1\bar{1}\bar{1})$ ***and*** $(\mathbf{1\bar{1}\bar{1}})$ ***surfaces. The arrow points from the unminimized structure to the energy minimized structure***

Additional Modeling Projections of Maleic Anhydride Over Tetracene (side view)

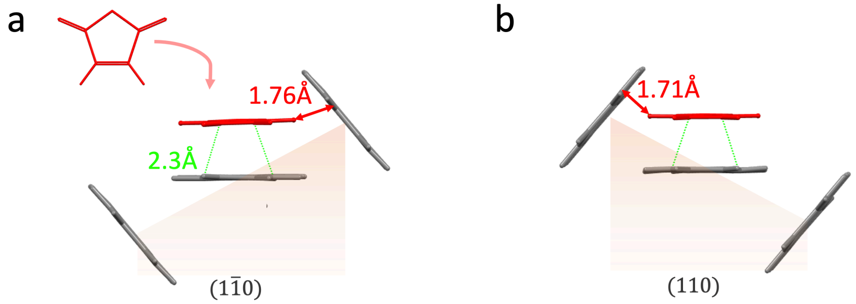

Figure S4: *For the measurements, the maleic anhydride was placed at the transition state above one of the more reactive center rings. Our model of steric effect begin with the expected transition state transition state for this Diels-Alder reaction places the maleic anhydride molecule parallel to the tetracene molecule ~2.3 Å apart for effective overlap of the π system. Assuming a comparable distance is necessary for reaction at the confined surfaces, the reaction cavities in this system can be simply modeled by placing the maleic anhydride at the transition state distance and calculating the distance to the point of closest contact with the other tetracene molecules in the lattice (atom-to-atom). The red distance is the distance to the nearest neighbor atom.*

Additional Modeling Projections of Maleic Anhydride Over Tetracene (top view)

(110)

Ring 2

Closest Contact 1.659Å

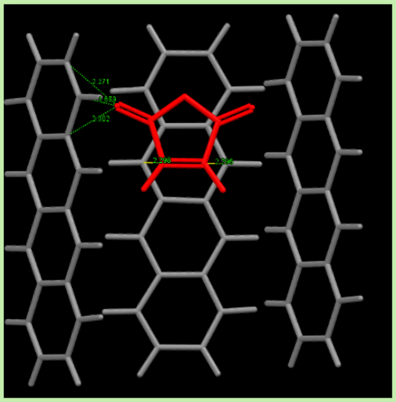

Closest H: 1.959Å

Closest Contact 1.712Å

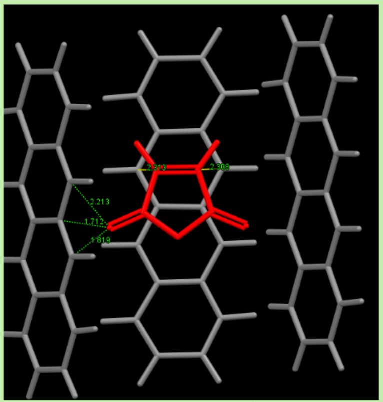

Closest H: 2.110Å

Ring 3

Closest Contact 1.623Å

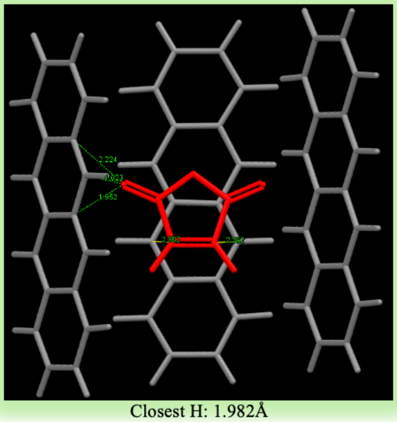

Closest H: 1.982Å

Closest Contact 1.682Å

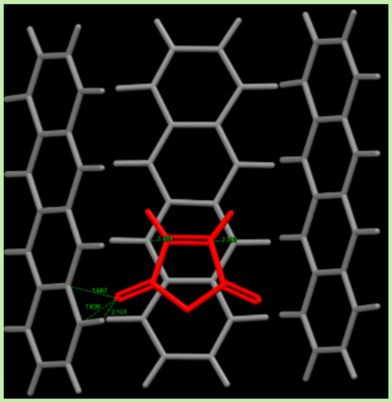

Closest H: 2.103Å

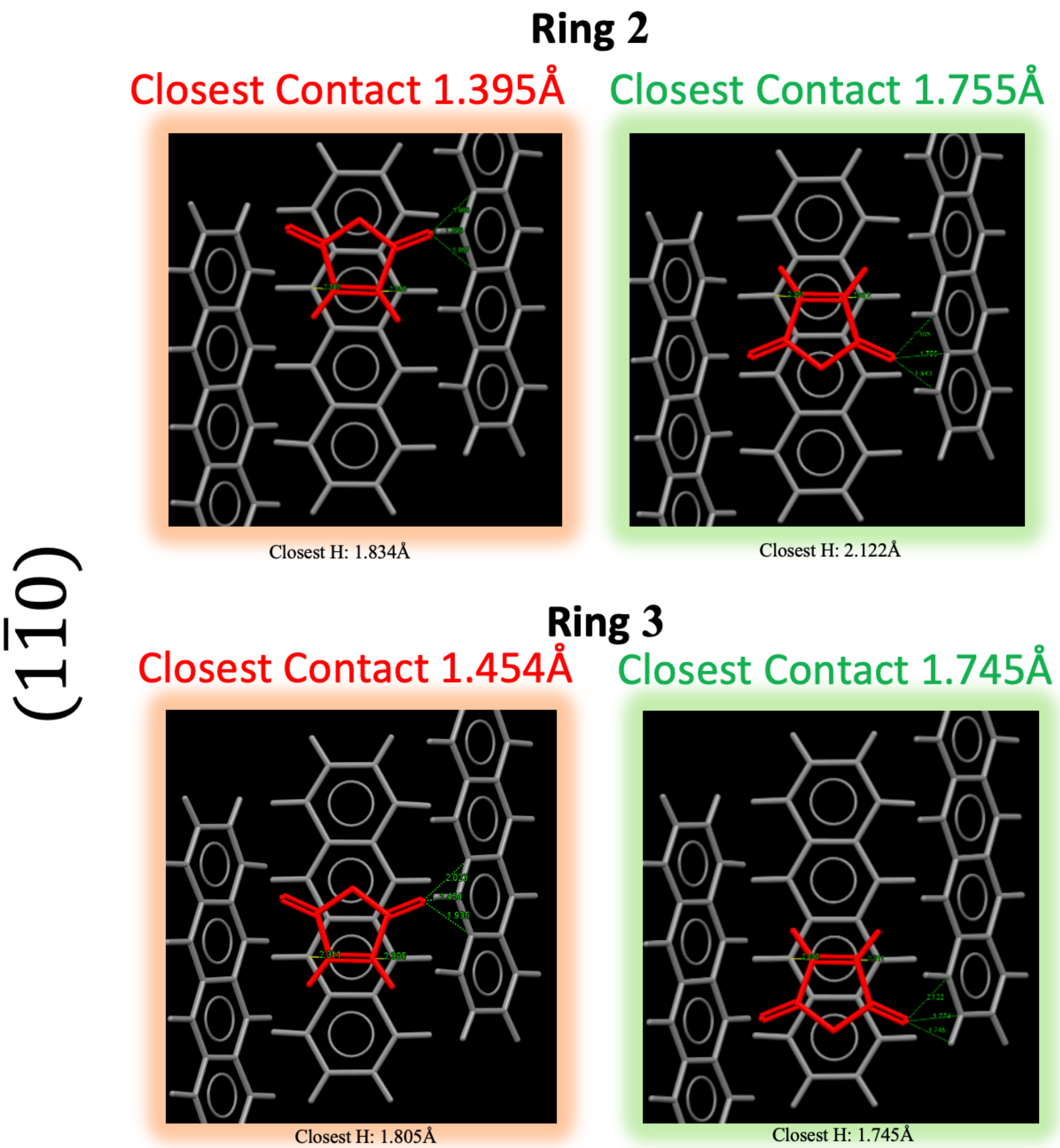

Figure S5: *Maleic anhydrides at each viable position for a Diels-Alder rection. Similar to Figure S4, the maleic anhydride molecule was placed parallel to the tetracene molecule ~2.3 Å apart. Distances to each of the nearest carbons on the tetracene rings are indicated in green, while the closest hydrogen is labeled under each image. From these, the closest contact for each position was determined and placed above each image.*

Path Traces for All Maleic Anhydrides Residing on the $(1\bar{1}0)$ Surface

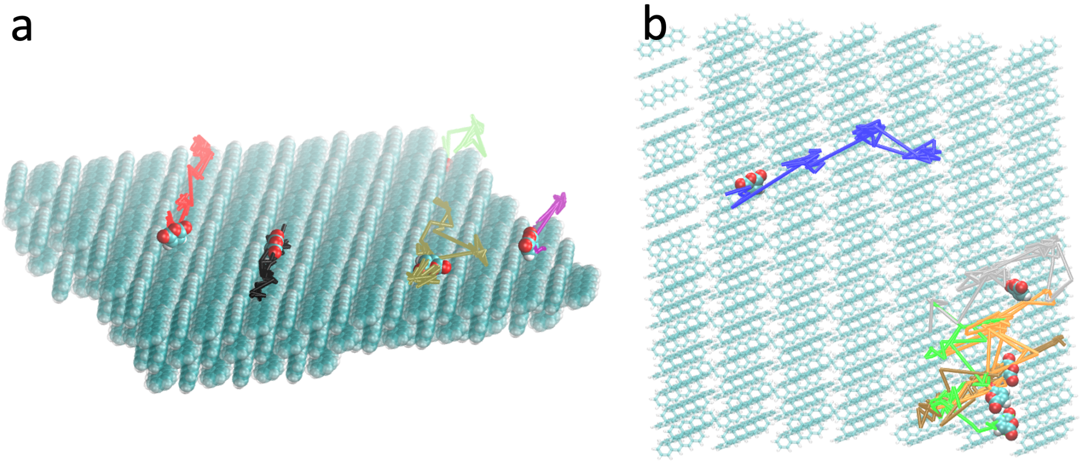

Figure S6: *Path traces of maleic anhydrides in the last half of the MD simulation on a* $(1\bar{1}0)$ *surface. (a) maleic anhydrides on the top of the surface. (b) Maleic anhydrides on the bottom of the surface.*

Path Traces for All Maleic Anhydrides Residing on the $(1\bar{1}\bar{1})$ Surface

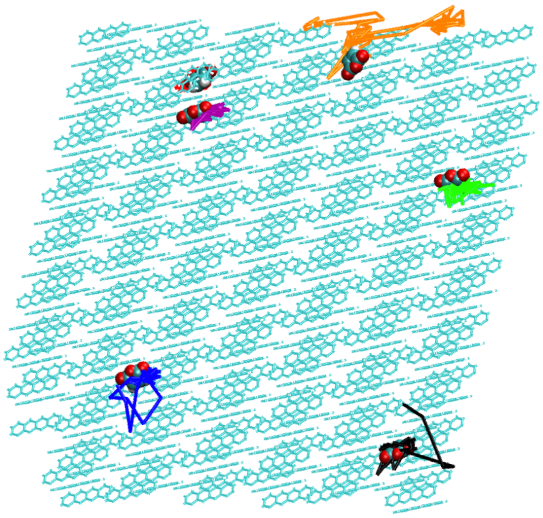

Figure S7: *Path traces of maleic anhydrides in the last half of the MD simulation on a* $(1\bar{1}\bar{1})$ *surface. Though individual maleic anhydrides ocassionally take time to find a cavity (e.g. blue trace) once they have entered, they remain in a single cavity.*

Path Traces for All Maleic Anhydrides Residing on the $(1\bar{1}1)$ Surface

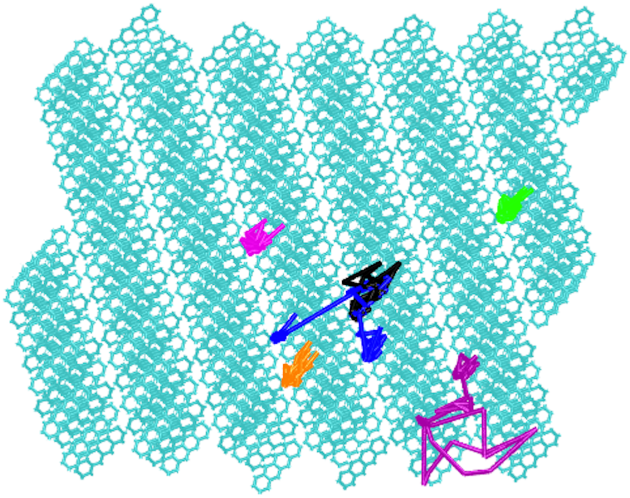

Figure S8: *Path traces of maleic anhydrides in the last half of the MD simulation on a $(1\bar{1}1)$ surface. Similar to the $(1\bar{1}\bar{1})$ surface, maleic anhydrides tend to remain in a cavity once they have entered. Note, the maleic anhydride resides towards the far end of the tetracene ring system (outer most ring).*

Path Traces for All Maleic Anhydrides Residing on the (110) Surface

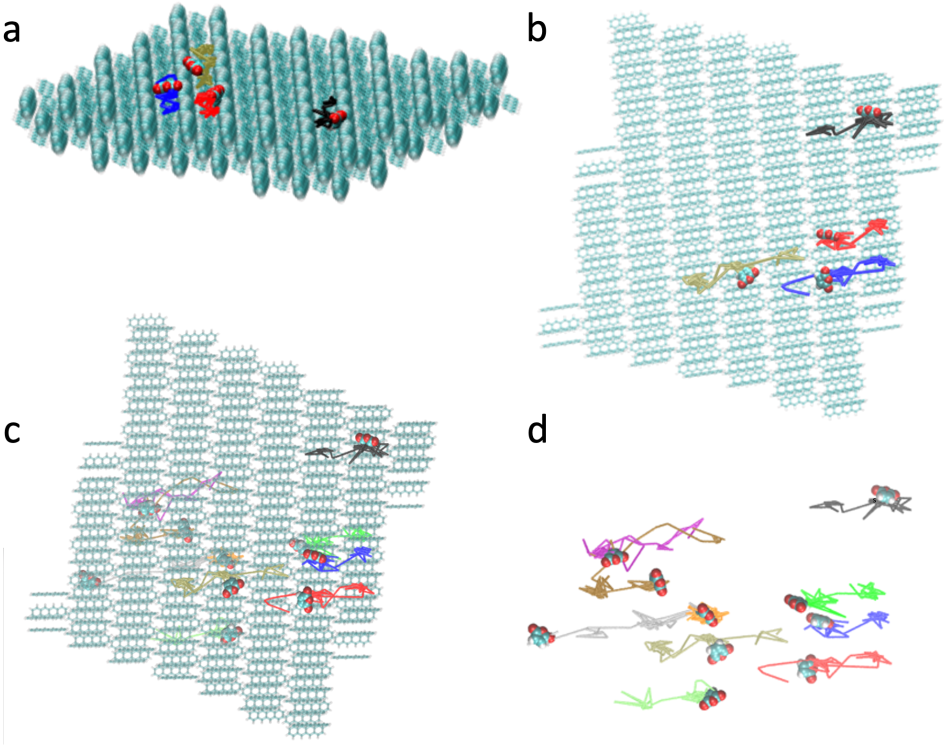

Figure S9: *Path traces of maleic anhydrides in the last half of the MD simulation on a (110) surface. (a,b) maleic anhydrides on the top of the surface. (c) Maleic anhydrides on the both sides of the surface. (d) Traces with the surface removed. The predominant path is along the channels formed by two tetracenes near surface normal on either side of tetracene near the plane of the surface.*

Path Traces for All Maleic Anhydrides Residing on the (100) Surface

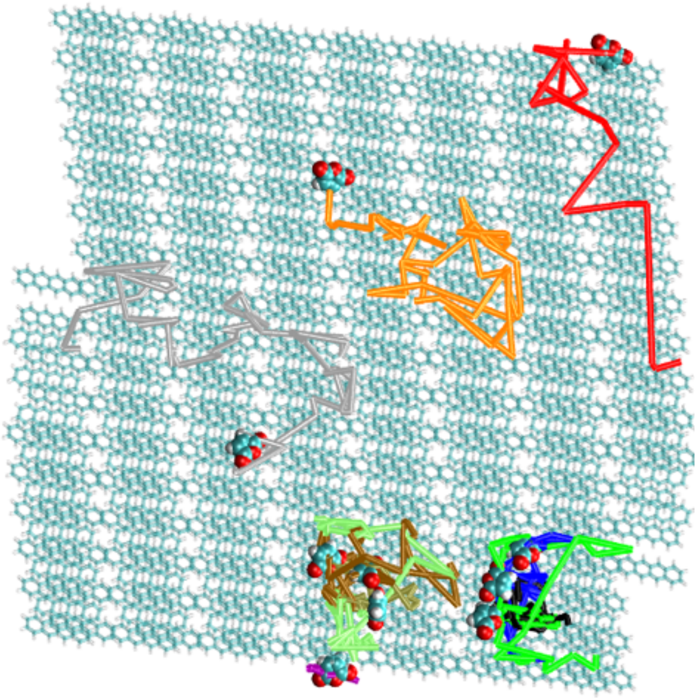

Figure S10: Path traces of maleic anhydrides in the last half of the MD simulation on a (100) *surface.*

Residence Time Analysis

Each individual maleic anhydride was tracked in each frame of the simulation for the number of frames it resided in a particular cavity on the surface. The molecules had minimal residence time across the (100) surface, not spending much time at all over a single site. The maleic anhydride does, however, stay relatively close to the surface defined by the (100) crystallographic plane, just like surfaces defined by the $(1\bar{1}0)$ and (110) crystallographic planes. The maleic anhydride molecules that entered the cavity in the (110) surface primarily stayed there, having an average residence time of *3.3 ns.* In the rare instances that they did leave the cavity, it tended to be a short distance translation before rapidly reentering the same cavity. In comparison, maleic anhydrides on the slower reacting $(1\bar{1}0)$ surface had a significantly lower residence time (*1.3 ns)*. For this surface the dominant maleic anhydride motion was movement from cavity to cavity, staying in one cavity for a short time before jumping to a nearby cavity. In these simulations, the (001) surface showed no maleic anhydride molecules reaching the reaction cavity (none within *7Å* of the reaction site). In fact, the low energy (001) surface showed so little interaction between the maleic anhydride and the exposed C-H bonds of tetracene that all the maleic anhydride molecules quickly left the surface. As described in the main text, maleic anhydrides for the $(1\bar{1}\bar{1})$ and $(1\bar{1}1)$ surfaces generally stayed in the cavity for the duration of the MD simulation once they had entered.

Additional Energy Minimizations

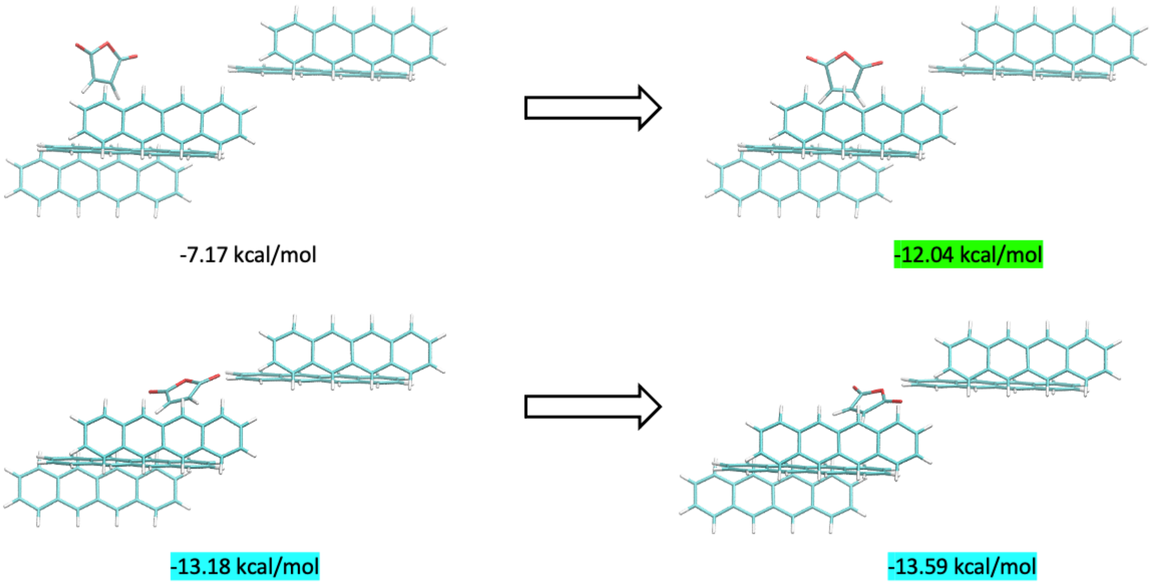

$(1\bar{1}1)$

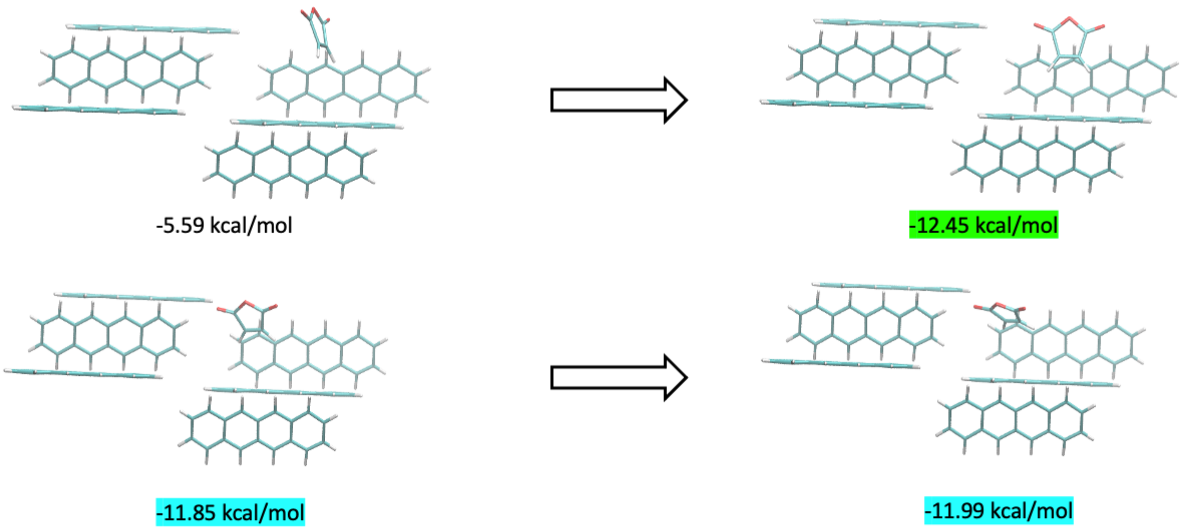

$(1\bar{1}\bar{1})$

Figure S11: *Several energy minimizations for the facets that differ in only the third index number. The arrow points from the unminimized structure to the energy minimized structure. All of the green highlighted energies demonstrate a low energy with the maleic anhydride in a poor reaction position. The blue highlighted energies also demonstrate a low energy, but these are twisted and tilted by the upper step molecule into a better reaction position.*

References

[1] J. Calimano, F. Li, J. Florián, D. M. Piñero-Cruz, T. R. Fielitz, R. J. Holmes, J. W. Ciszek, *J. Phys. Chem. C* 2020, **124**, 23716–23723.

[2] C. R. Groom, I. J. Bruno, M. P. Lightfoot, S. C. Ward, *Acta Crystallogr. Sect. B Struct. Sci. Cryst. Eng. Mater.* 2016, **72**, 171–179.

[3] C. F. Macrae, I. Sovago, S. J. Cottrell, P. T. A. Galek, P. McCabe, E. Pidcock, M. Platings, G. P. Shields, J. S. Stevens, M. Towler, P. A. Wood, *J. Appl. Crystallogr.* 2020, **53**, 226–235.

[4] W. Humphrey, A. Dalke, K. Schulten, *J. Mol. Graph.* 1996, **14**, 33–38.

[5] J. C. Phillips, R. Braun, W. Wang, J. Gumbart, E. Tajkhorshid, E. Villa, C. Chipot, R. D. Skeel, L. Kalé, K. Schulten, *J. Comput. Chem.* 2005, **26**, 1781–1802.

[6] K. Vanommeslaeghe, E. Hatcher, C. Acharya, S. Kundu, S. Zhong, J. Shim, E. Darian, O. Guvench, P. Lopes, I. Vorobyov, A. D. Mackerell Jr., *J. Comput. Chem.* 2010, *31*, 671–690.

[7] R. B. Best, X. Zhu, J. Shim, P. E. M. Lopes, J. Mittal, M. Feig, A. D. MacKerell, *J. Chem. Theory Comput.* 2012, **8**, 3257–3273.

[8] A. D. MacKerell, M. Feig, C. L. Brooks, *J. Am. Chem. Soc.* 2004, **126**, 698–699.

[9] A. D. MacKerell, D. Bashford, M. Bellott, R. L. Dunbrack, J. D. Evanseck, M. J. Field, S. Fischer, J. Gao, H. Guo, S. Ha, D. Joseph-McCarthy, L. Kuchnir, K. Kuczera, F. T. K. Lau, C. Mattos, S. Michnick, T. Ngo, D. T. Nguyen, B. Prodhom, W. E. Reiher, B. Roux, M. Schlenkrich, J. C. Smith, R. Stote, J. Straub, M. Watanabe, J. Wiórkiewicz-Kuczera, D. Yin, M. Karplus, *J. Phys. Chem. B* 1998, **102**, 3586–3616.